

## TOPICAL REVIEW

# Spin-1 pyrochlore antiferromagnets: Theory, model, and materials' survey

Yong-Hao Gao<sup>1,\*</sup>, Xu-Ping Yao<sup>2,\*</sup>, Fei-Ye Li<sup>1,\*</sup>, Gang Chen<sup>2,†</sup>

<sup>1</sup>State Key Laboratory of Surface Physics and Department of Physics, Fudan University, Shanghai 200433, China

<sup>2</sup>Department of Physics and HKU-UCAS Joint Institute for Theoretical and Computational Physics at Hong Kong,

The University of Hong Kong, Hong Kong, China

Corresponding author. E-mail: <sup>†</sup>gangchen@hku.hk

Received November 19, 2019; accepted June 13, 2020

Pyrochlore magnets can be a unique platform to demonstrate numerous important concepts and applications of frustrated magnetic physics in modern condensed matter physics. Most works on pyrochlore magnets deal with the interacting spin-1/2 local moments, while much less works have studied the spin-1 systems. We here review the physics with interacting spin-1 local moments on the pyrochlore lattice to illustrate the potentially interesting physics associated with spin-1 magnets. The generic pyrochlore spin-1 model includes the antiferromagnetic Heisenberg interaction, the Dzyaloshinskii–Moriya interaction and the single-ion spin anisotropy. The global phase diagram of this generic spin model is reviewed, and the relation between different quantum phases in the phase diagram is clarified. The critical properties of the transition from the parent quantum paramagnet to the proximate orders are discussed. The presence of quantum order by disorder in the parts of the ordered phases is analyzed. The elementary excitations with respect to the ground states are further reviewed, and the topological natures of these excitations are carefully addressed. The materials' relevance of the spin-1 pyrochlore magnets are finally reviewed. This review may provide insights about the interesting spin-1 local moments on frustrated systems.

**Keywords** topological magnon, quantum order by disorder, Dzyaloshinskii–Moriya interaction, flavor wave theory

### Contents

1	Introduction
2	Model Hamiltonian
3	Flavor wave theory for quantum paramagnet
3.1	Flavor wave representation
3.2	Ideas of linear flavor wave theory
3.3	Critical properties from flavor wave theory
4	Mean-field theory
4.1	All-in all-out AFM
4.2	Splayed FM
4.3	Coplanar XY AFM <sub>1</sub>
4.4	Coplanar XY AFM <sub>2</sub>
4.5	Non-coplanar XY AFM
4.6	Topological magnons and spin wave excitations of the ordered phases
5	Summary with a materials' survey
	Acknowledgements
	References

many ways [1–9]. In the field of frustrated magnetism, there has been a growing interest and effort in the systems with interacting spin-1 local moments where interesting quantum phases and unconventional excitations have been predicted for frustrated spin-1 Mott insulators [1–9]. In particular, a chiral liquid phase with a finite vector chirality order has been obtained for the spin-1 triangular lattice magnet [8], Haldane phase like symmetry-protected topological phases have been suggested for three-dimensional spin-1 systems [5, 10], spin liquid related physics and phenomenology has been explored for the layered triangular material Ba<sub>3</sub>NiSb<sub>2</sub>O<sub>9</sub> [11–17], and exotic excitations with degenerate band minima were established for the spin-1 diamond lattice antiferromagnet [6, 9].

The pyrochlore antiferromagnet [18] is a stereotype of spin systems with geometrical frustration and numerous quantum phases, and many interesting ideas and applications of quantum frustrated magnetism can be directly applied. In the last decade or so, most efforts in the field were devoted to the rare-earth pyrochlore magnets where the relevant degrees of freedom are certain spin–orbital-entangled effective spin-1/2 local moments [18–63]. Due to the geometrical frustration and the bond-dependent anisotropic spin interaction [19, 20, 25, 64, 65], intriguing magnetic phases and phenomena, quantum spin ice and U(1) quantum spin liquid for example, have been proposed

## 1 Introduction

Interacting spin-1 magnetic systems are believed to be fundamentally different from their spin-1/2 counterparts in

\*These authors contributed equally.  
 Corresponding Editor: Nan-Lin Wang.

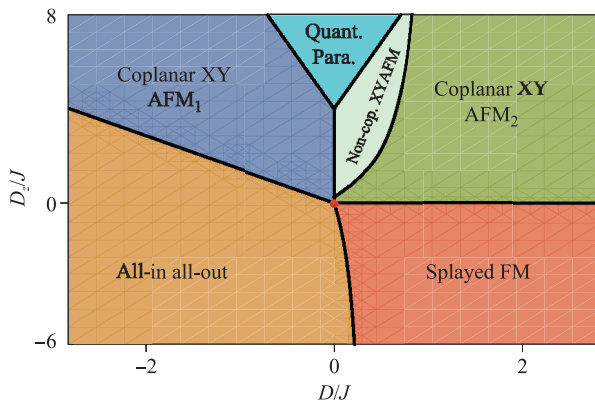


**Fig. 1** The phase diagram of our generic spin model for the spin-1 pyrochlore system. Here, the Heisenberg exchange  $J$  is set to be antiferromagnetic with  $J > 0$ . “Quant. Para.” refers to the quantum paramagnetic phase. The details of the ordered phases are explained in the main text. The (red) dot is the Heisenberg point of the model.

and widely explored [22, 25–27]. This field is fertilized by the existence of the abundant rare-earth pyrochlore magnets with different magnetic ions. There are emerging efforts on interacting local moments with  $3d$  transition metal ions on the pyrochlore lattice, and a new family of fluoride pyrochlore systems with the transition metal ions  $\text{Fe}^{2+}$ ,  $\text{Co}^{2+}$ ,  $\text{Ni}^{2+}$  and  $\text{Mn}^{2+}$  has been synthesized [66–69]. Unlike the rare-earth  $4f$  electrons whose interactions are usually quite small, these new systems, consisting of transition metal ions, have much stronger spin interactions. Moreover, spin–orbit coupling is less important in these systems, although spin–orbit coupling sometimes becomes active and modifies the local moment structure if there exists a partially filled  $t_{2g}$  shell for the magnetic ions [70], and these systems sometimes support interacting spin-1 local moments instead of effective spin-1/2 moments. Given the limited works on spin-1 pyrochlore magnets, this short review is not supposed to be quite comprehensive, but instead is hoped to provide more on physical insights and motivations.

Just like the fundamental distinction between the half-integer and the integer spin moments for one dimensional spin chains that was pointed out by Haldane [1, 2], the physical properties of the half-integer spin and the integer spin moments on the pyrochlore lattice are expected to be quite different. In fact, for the rare-earth pyrochlore magnets, such a distinction has already been manifested in the Kramers doublet system and the non-Kramers doublet system where the non-Kramers doublet originates from integer spin and supports magnetic quadrupolar order [25, 27, 33]. Since most works in this field are dealing with effective spin-1/2 pyrochlores, it is valuable to analyze the generic physics of the spin-1 pyrochlores. Among the existing fluoride pyrochlores,  $\text{Co}^{2+}$  and  $\text{Mn}^{2+}$  have half-integer spin moments while the  $\text{Ni}^{2+}$  and  $\text{Fe}^{2+}$  ions have integer spin moments [66–69]. From the conventional wisdom, when the spin moment is large, the sys-

tem tends to behave more classically. For geometrically frustrated systems, however, the spin-1 local moments could occasionally give rise to quantum phenomena. Indeed, in the Ni-based fluoride pyrochlore  $\text{NaCaNi}_2\text{F}_7$ , spin-ordering-related features were not found in the thermodynamic measurements down to the spin glassy transition at 3.6 K that is attributed to the possible bond randomness, although the system has the Curie–Weiss temperature  $-129$  K [66]. Apart from this new material, the spin-1 pyrochlore magnets have already been suggested for the Ru-based pyrochlore  $\text{A}_2\text{Ru}_2\text{O}_7$  and the Mo-based pyrochlore  $\text{A}_2\text{Mo}_2\text{O}_7$ , despite the fact that the stronger spin–orbit coupling of the  $4d$  electrons can be more important in these two systems. Partly motivated by these experiments and more broadly about the physics of the spin-1 moments, we review the generic spin model and the magnetic properties of the spin-1 local moments on the pyrochlore lattice.

In addition to the Heisenberg model that is usually assumed for the  $3d$  transition metal ions and sometimes for the  $4d$  transition metal ions, there exist the on-site single-ion spin anisotropy and the antisymmetric Dyzalooshinskii–Moriya interaction. The phase diagram for interacting spin-1 pyrochlore magnets is summarized in Fig. 1. To illustrate the thought, one starts from the quantum paramagnetic ground state in the strong single-ion spin anisotropic limit and explores the instability of this quantum state as the Heisenberg exchange and the Dyzalooshinskii–Moriya interaction are switched on. Mostly relying on a flavor wave theory, one can access the phase transitions out of this quantum paramagnetic state and explore the properties of criticalities. Inside the ordered phases, we implement the usual mean-field theory and establish the phase diagram on the ordered side. One can further identify the region on the ordered side where there exist continuous degeneracies of the ground state manifold at the mean-field level. The quantum fluctuation is studied and lifts the continuous degeneracies. The magnetic excitations in different phases are also discussed.

The following parts of this review are organized as follows. In Section 2, we explain the generic spin-1 model Hamiltonian. In Section 3, we explain the flavor wave theory, and explore the magnetic excitation and the instability of the quantum paramagnetic phase. In Section 4, we focus on the ordered side and explain the magnetic properties of the magnetic orders. Finally in Section 5, we summarize the theoretical side and the physical properties of the phase diagram, and review the materials’ relevance of the spin-1 pyrochlore magnets.

## 2 Model Hamiltonian

We start the review from explaining the local moment physics of the  $\text{Ni}^{2+}$  ion in  $\text{NaCaNi}_2\text{F}_7$ . Although the starting point here is specific to  $\text{NaCaNi}_2\text{F}_7$ , the physi-

cal model itself applies broadly to other spin-1 pyrochlore systems, and we merely present the model through the specific case of  $\text{NaCaNi}_2\text{F}_7$ . The  $\text{Ni}^{2+}$  ion has a  $3d^8$  electron configuration. In the octahedral crystal field environment of  $\text{NaCaNi}_2\text{F}_7$ , the six electrons occupy the lower  $t_{2g}$  orbitals, and the remaining two electrons occupy the upper  $e_g$  orbitals and form a spin  $S = 1$  local moment. There is no orbital degeneracy here. The following spin model was proposed for the interaction between the local moments [71]. The minimal spin Hamiltonian is given as

$$H = \sum_{\langle ij \rangle} [J\mathbf{S}_i \cdot \mathbf{S}_j + \mathbf{D}_{ij} \cdot (\mathbf{S}_i \times \mathbf{S}_j)] + \sum_i D_z (\mathbf{S}_i \cdot \hat{z}_i)^2, \quad (1)$$

where  $\mathbf{D}_{ij}$  is the bond-dependent vector that defines the antisymmetric Dzyaloshinskii–Moriya interaction [72]. For the 01 bond in Fig. 2(a), one has  $\mathbf{D}_{01} = (0, D/\sqrt{2}, -D/\sqrt{2})$ , and  $\mathbf{D}_{ij}$ 's on other bonds are readily obtained from the lattice symmetry. The  $D_z$  term is the single-ion spin anisotropy allowed by the  $D_{3d}$  point group symmetry of the pyrochlore lattice, and  $\hat{z}_i$  is the local  $\langle 111 \rangle$  axis that is defined locally for each pyrochlore sublattice. Even though the Dzyaloshinskii–Moriya interaction arises from the first order effect of the spin–orbit coupling and the single-ion spin anisotropy arises from the second order effect of the spin–orbit coupling, it does not necessarily indicate the single-ion anisotropy is weaker than the Dzyaloshinskii–Moriya interaction. In fact, ignoring the effect from Hund's coupling, one has the following results [73]:

$$|D_{ij}|/J \sim \mathcal{O}(\lambda/\Delta), \quad (2)$$

$$|D_z|/\Delta \sim \mathcal{O}(\lambda^2/\Delta^2), \quad (3)$$

where  $\lambda$  is the spin–orbit coupling and  $\Delta$  is the crystal electric field splitting between the  $t_{2g}$  and the  $e_g$  manifolds and can be much larger than the superexchange interaction  $J$ . As a result, whether  $\lambda$  appears as the linear order or as the second order cannot be used to argue for the relative magnitudes of  $|D_{ij}|$  and  $D_z$ . Both couplings are

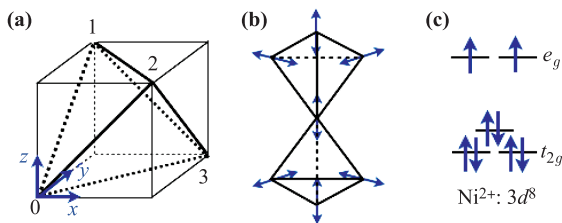


**Fig. 2** (a) The four sublattices and the unit cell of the pyrochlore lattice. (b) The (blue) arrows define the local  $z$  or  $\langle 111 \rangle$  axis. (c) The electron configuration of the  $\text{Ni}^{2+}$  ion in  $\text{NaCaNi}_2\text{F}_7$ . While the  $e_g$  orbitals remain degenerate under the  $D_{3d}$  point group, the  $t_{2g}$  orbitals would be broken into  $a_{1g}$  and two-fold degenerate  $e'_g$  orbitals. The relative energies of  $a_{1g}$  and  $e'_g$  orbitals are unknown, and  $a_{1g}$  is placed at a higher energy in the figure. The  $S = 1$  nature of the  $\text{Ni}^{2+}$  local moment holds for either distribution of the  $a_{1g}$  and  $e'_g$  orbitals.

included in the model Hamiltonian. The pseudo-dipolar interactions were neglected, as they are subleading compared to the Dzyaloshinskii–Moriya interaction for the  $3d$  transition metal ions without any orbital degeneracy. The pseudo-dipolar interactions, however, may become important for the  $4d$  transition metal ions.

### 3 Flavor wave theory for quantum paramagnet

The generic spin model contains three different interactions. The quantum ground state of the Heisenberg model is one of the hardest problems in quantum magnetism, so it is not so profitable to start from there. Instead, one starts from the strong single-ion spin anisotropy limit with  $D_z > 0$  where the ground state is a simple product state of the quantum paramagnet with

$$|\text{quantum paramagnet}\rangle = \prod_i |S_i^z \equiv \mathbf{S}_i \cdot \hat{z}_i = 0\rangle. \quad (4)$$

This state is impossible for the half-integer spin local moments as there is always Kramers' degeneracy. From this well-understood limit, one turns on the exchange interaction and study the evolution of the magnetic excitation and the instability.

#### 3.1 Flavor wave representation

This quantum paramagnet has no long-range magnetic order, and the conventional Holstein–Primarkoff spin-wave theory cannot be directly applied at all. For the purpose, one invokes so-called flavor wave theory, that was first developed in Ref. [74] for the  $SU(4)$  spin–orbital model [75], and properly adjusts the formulation to the current case. One defines the states in the spin-1 local moment Hilbert space as

$$|m\rangle_i \equiv |S_i^z = m\rangle, \quad (5)$$

with  $m = 0, \pm 1$ , and introduces three flavors of the boson operators  $a_m^\dagger(i)$  to represent the spin operators  $S_i^\alpha$  as  $a_m^\dagger(i)\langle m|S^\alpha|n\rangle a_n(i)$ , with  $\alpha = x, y, z$ . For the quantum paramagnet, one condenses  $a_0^\dagger(i)$  and  $a_0(i)$  to  $\bar{a}_i$ , with

$$\bar{a}_i = \left[1 - a_1^\dagger(i)a_1(i) - a_{-1}^\dagger(i)a_{-1}(i)\right]^{1/2}. \quad (6)$$

Thus one has two flavors of the boson operators remained and  $a_1^\dagger(i), a_{-1}^\dagger(i)$  create magnetic excitation from  $|0\rangle_i$  to  $|1\rangle_i, |-1\rangle_i$ , respectively. This is very different from the usual Holstein–Primakoff transformation where only one boson is introduced to describe the quantum fluctuation of the magnetic order. The underlying reason is due to the particular form of the Hamiltonian and the quantum paramagnetic ground state that allow the excitations of the  $|1\rangle_i, |-1\rangle_i$  states to be equally important. As a consequence, the excitation spectra for this quantum paramagnet should have eight bands, rather than the four bands

in the usual Holstein–Primakoff spin wave theory. Moreover, since the model has no continuous symmetry, the magnetic excitations should be fully gapped.

### 3.2 Ideas of linear flavor wave theory

To carry out the actual calculation of the excitation spectra, one replaces the physical spin operators using the flavor wave transformation and keeps the Hamiltonian to the quadratic orders in the boson operators to obtain a linear flavor wave theory Hamiltonian [71].

In Figs. 3(a) and (b), we plot the linear flavor wave dispersion for the specific choices of the couplings within the quantum paramagnetic phase. As we expect, there are eight bands of the magnetic excitations that are fully gapped. Besides the doubled number of the bands, we notice other unusual properties of the excitations. One found that, in the  $D < 0$  region of the quantum paramagnetic phase, the minima of the magnetic excitations develop a line of degeneracies from  $\Gamma$  to L in the momentum space and a threefold degeneracy in the spin space at the  $\Gamma$  point. In the  $D > 0$  region of the quantum paramagnetic phase, the band minima of the two lowest bands touch at the  $\Gamma$  point with an accidental two-fold degeneracy in the spin space. Both the momentum space degeneracy and the spin space degeneracy are not protected by any symmetry of the spin Hamiltonian. We expect the emergent degeneracy to be lifted when we go beyond the linear flavor wave theory and include the interaction between the flavor bosons.

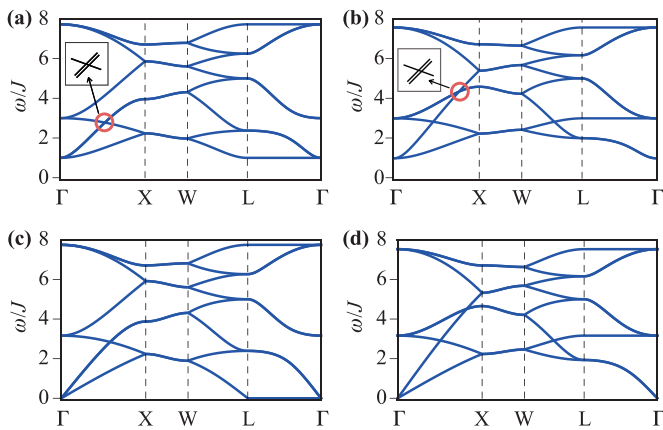


**Fig. 3** (a, b) The (gapped) magnetic excitations in the quantum paramagnetic phase. (c, d) The magnetic excitations on the phase boundary of the quantum paramagnet with the excitation gap closed. The parameters are (a)  $D = -0.14J, D_z = 5J$ ; (b)  $D = 0.14J, D_z = 5J$ ; (c)  $D = -0.17J, D_z = 5J$ ; (d)  $D = 0.17J, D_z = 5J$ . The high symmetry momenta are  $\Gamma = (0, 0, 0)$ ,  $X = (0, 2\pi, 0)$ ,  $W = (\pi, 2\pi, 0)$ ,  $L = (\pi, \pi, \pi)$ . It is ready to observe the existence of the triply degenerate nodes (red circle) in the spectrum [71]. In the insets of (a) and (b), the two-fold degenerate bands are split artificially for demonstration.

### 3.3 Critical properties from flavor wave theory

As one further increases the exchange interaction from the quantum paramagnet, the gap of the magnetic excitations gradually diminishes. Eventually, as the gap is closed, phase transition happens and the system develops magnetic orders. To explain the critical properties, one can examine the transition from the flavor wave theory. In the  $D < 0$  region, the degenerate modes along the momentum line from  $\Gamma$  to L become critical at the same time as the gap is closed, see Fig. 3(c). Because of the line degeneracy, there is an enhanced density of states at low energies at the criticality, and one would expect the specific heat  $C_v \sim T^2$  behavior at low temperatures from the mean-field theory. The zero-temperature limit of the specific heat should be modified because the fluctuations break the momentum space degeneracy and lead to a discrete degeneracy. In the  $D > 0$  region, as the system approaches the criticality, only the  $\Gamma$  point becomes critical, see Fig. 3(d), and one expects a simple  $C_v \sim T^3$  at the mean-field level and a logarithmic correction when the fluctuations beyond the mean-field are included.

The critical modes also contain information on the proximate magnetic orders out of the quantum paramagnetic phase, which is discussed and compared with the mean-field theory from the ordered phase side [71].

## 4 Mean-field theory

To study the proximate magnetic orders out of the quantum paramagnetic phase, one natural approach would simply follow the flavor wave theory that was introduced in the previous section and study the condensation of the critical flavor wave modes. This is certainly feasible and requires including the interactions between the flavor wave modes that lift the degeneracy of the low-energy modes. One, however, can implement a mean-field theory to understand the physics here. This is justified since the system develops magnetic orders in the interesting parameter regimes. This mean-field approach works best deep on the ordered side. In the mean-field theory, one simply replaces the spin operator with the mean-field spin order parameter and optimize the mean-field Hamiltonian,

$$\begin{aligned} \langle H \rangle = & \sum_{\langle ij \rangle} [J \mathbf{m}_i \cdot \mathbf{m}_j + \mathbf{D}_{ij} \cdot (\mathbf{m}_i \times \mathbf{m}_j)] \\ & + \sum_i D_z (\mathbf{m}_i \cdot \hat{z}_i)^2, \end{aligned} \quad (7)$$

under the local constraint  $|\mathbf{m}_i|^2 = S^2$ . The mean-field ground state can then be found using the simple Luttinger–Tisza method. Our results are summarized and displayed in Fig. 1 and Fig. 4. All of these orders support an ordering wavevector  $\mathbf{Q} = \mathbf{0}$  where the magnetic unit cell coincides with the crystal unit cell. In the following, we describe the magnetic orders in details. Since the mag-

netic orders are focused here, the results will be presented from bottom to top and from left to right in the phase diagram of Fig. 1.

#### 4.1 All-in all-out AFM

In the lower left region of the phase diagram, the “all-in all-out” magnetic order is stabilized. This is understood as follows. The easy-axis anisotropy favors the spins to be aligned with the local  $\hat{z}$  direction, and the Heisenberg interaction requires the vector addition of the spins from the four sublattices to be zero. The Dzyaloshinskii–Moriya interaction is less obvious, but naturally favors non-collinear spin configurations. Simple diagonalization of the Dzyaloshinskii–Moriya interaction term directly gives the “all-in all-out” spin configuration. Therefore, all three interactions in the Hamiltonian are optimized by the “all-in all-out” spin configuration. This “all-in all-out” state extends further into the easy-plane anisotropic regime with  $D_z > 0$ . As the local  $\hat{z}$  direction is a three-fold rotational axis, this symmetry operation does not generate new ground states, and the ground state spin configuration merely has a  $\mathbb{Z}_2$  degeneracy from the time-reversal transformation.

#### 4.2 Splayed FM

In the lower right region of the phase diagram, the “splayed ferromagnet” (“splayed FM”) is stabilized. One such spin configuration is given in Fig. 4(b) and parameterized as

$$\begin{cases} \mathbf{m}_0 = \left( \frac{\sin \alpha}{\sqrt{2}}, \frac{\sin \alpha}{\sqrt{2}}, \cos \alpha \right), \\ \mathbf{m}_1 = \left( -\frac{\sin \alpha}{\sqrt{2}}, \frac{\sin \alpha}{\sqrt{2}}, \cos \alpha \right), \\ \mathbf{m}_2 = \left( \frac{\sin \alpha}{\sqrt{2}}, -\frac{\sin \alpha}{\sqrt{2}}, \cos \alpha \right), \\ \mathbf{m}_3 = \left( -\frac{\sin \alpha}{\sqrt{2}}, -\frac{\sin \alpha}{\sqrt{2}}, \cos \alpha \right), \end{cases} \quad (8)$$

where  $\mathbf{m}_\mu$  refers to the magnetic order on the  $\mu$ -th sublattice, and the “splay angle”  $\alpha$  is found to be  $\alpha = \arctan[D'_z - (8D_z^2 + D_z'^2)^{\frac{1}{2}} / (2\sqrt{2}D_z)]$ , with  $D'_z \equiv D_z - 12J - 3\sqrt{2}D$ . There is a ferromagnetic com-

ponent  $\cos \alpha$  along the global  $\hat{z}$  direction.

Other equivalent ground state spin configurations can be obtained by lattice symmetry operations. Together with the time reversal symmetry, there exists a  $\mathbb{Z}_3 \times \mathbb{Z}_2$  degeneracy. This state supports a weak ferromagnetism along one cubic axis and antiferromagnetism in the remaining two directions. Clearly, when  $|D_z|$  is dominant, the spins should be aligned with the local  $\hat{z}$  direction, and the Dzyaloshinskii–Moriya interaction then favors “two-in two-out” spin configurations in this case. In contrast, in the weak  $D_z$  limit, one has  $\alpha = 90^\circ$  and the ground state becomes coplanar. This means the “two-in two-out” spin ice configurations are smoothly connected to coplanar states in this “splayed FM” regime.

#### 4.3 Coplanar XY AFM<sub>1</sub>

In the upper left region of the phase diagram, one obtains a coplanar antiferromagnetic spin ground state and dubs it “coplanar XY AFM<sub>1</sub>”. Here “XY” refers to the  $xy$  plane of the local coordinate system. One such spin state is depicted in Fig. 4(c) and is given as

$$\begin{cases} \mathbf{m}_0 = \frac{1}{\sqrt{2}}(1, \bar{1}, 0), \\ \mathbf{m}_1 = \frac{1}{\sqrt{2}}(\bar{1}, \bar{1}, 0), \\ \mathbf{m}_2 = \frac{1}{\sqrt{2}}(1, 1, 0), \\ \mathbf{m}_3 = \frac{1}{\sqrt{2}}(\bar{1}, 1, 0). \end{cases} \quad (9)$$

The spins are perpendicular to the local  $\hat{z}$  direction of the relevant sublattice and orient antiferromagnetically within the same plane globally. This explains the use of the “coplanar XY AFM<sub>1</sub>”. This “coplanar XY AFM<sub>1</sub>” ground state occurs when  $D_z > \sqrt{2}|D|$  as one further increases the easy-plane anisotropy from the “all-in all-out” phase. This “coplanar XY AFM<sub>1</sub>” phase is in the easy-plane anisotropic limit, and the spins prefer to orient in the local  $xy$  plane. The in-plane spin configuration is able to content both the easy-plane spin anisotropy and the Heisenberg exchange but not the Dzyaloshinskii–Moriya interaction. This particular spin configuration of the “coplanar XY AFM<sub>1</sub>” state is obtained because the easy-

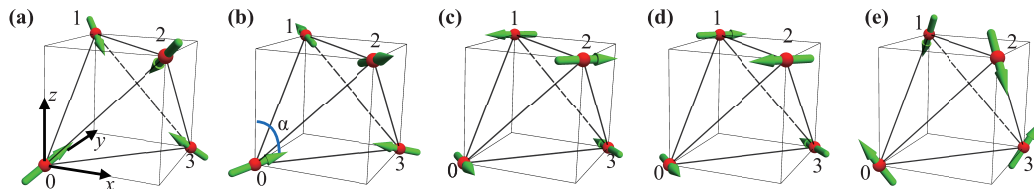


**Fig. 4** Representative configurations of the magnetic ordered phases in the phase diagram of Fig. 1. (a) All-in-all-out. (b) Splayed FM. The splay angle is labeled by  $\alpha$ . For this configuration,  $\alpha = 74.2^\circ$ . (c) Coplanar XY AFM<sub>1</sub>. (d) Coplanar XY AFM<sub>2</sub>. (e) Non-coplanar XY AFM.

plane anisotropy wins over the Dzyaloshinskii–Moriya interaction, such that the Dzyaloshinskii–Moriya interaction is optimized within the manifold of coplanar spin configurations only.

Again we have a  $\mathbb{Z}_3 \times \mathbb{Z}_2$  degeneracy for the ground state from the lattice symmetry and the time reversal symmetry operations. In the literature on quantum spin ice, the same classical state is referred to as “Palmer–Chalker” state or “ $\Psi_4$ ” state [76, 77].

#### 4.4 Coplanar XY AFM<sub>2</sub>

In the upper right region (both the “coplanar XY AFM<sub>2</sub>” and “non-coplanar XY AFM”) of the phase diagram, one found an extensively degenerate mean-field ground state, and all the three interactions are optimized at the same time. The extensive degeneracy is parametrized by a  $U(1)$  angular variable  $\theta$ , and the ground state spin configuration is given as

$$\mathbf{m}_\mu = \hat{x}_\mu \cos \theta + \hat{y}_\mu \sin \theta, \quad (10)$$

with  $\theta \in [0, 2\pi)$ . The generic spin Hamiltonian does not have any continuous symmetry, thus the continuous degeneracy is not the symmetry property of the Hamiltonian but is accidental, and can be lifted by the quantum fluctuation. This quantum order by disorder effect has been previously explored in the effective spin-1/2 pyrochlore material  $\text{Er}_2\text{Ti}_2\text{O}_7$  [78–80]. Here, quantum fluctuation picks  $\theta = n\pi/3 + \pi/6$  for  $n \in \mathbb{Z}$ , in the phase dubbed as “coplanar XY AFM<sub>2</sub>”. One such spin configuration is displayed in Fig. 4(d), and all the spins orient antiferromagnetically within the same plane. The same classical state is referred to as “ $\Psi_3$ ” state in the literature on quantum

spin ice [77].

#### 4.5 Non-coplanar XY AFM

In the remaining part of the upper right region in the phase diagram, quantum fluctuation leads to different ground state spin configurations, i.e., the quantum fluctuation selects  $\theta = n\pi/3$  for  $n \in \mathbb{Z}$ . One such spin configuration is displayed in Fig. 4(e), and all the spins orient antiferromagnetically but are not in the same plane. This phase is dubbed “non-coplanar XY AFM”. The same classical state is referred to as “ $\Psi_2$ ” state in the literature on quantum spin ice [77]. The detailed calculation of the order by quantum disorder effect can be found in Ref. [71].

#### 4.6 Topological magnons and spin wave excitations of the ordered phases

In Fig. 5, the spin wave excitation of each ordered phase is plotted along high symmetry lines in the Brillouin zone. As expected, the spectra in Figs. 5(a)–(c) are fully gapped while in Figs. 5(d) and (e), there are gapless pseudo-Goldstone modes at the  $\Gamma$  point, reflecting the continuous  $U(1)$  degeneracy in the mean-field ground state manifold. Since the degeneracy is accidental, a small gap is expected when we go beyond the linear spin wave approximation.

We further explain the topological spin wave modes in the spectrum. Besides the Weyl nodes (see Fig. 6), we find extra doubly degenerate band touchings, labeled by green circles in Fig. 5. These touchings belong to certain nodal lines (see Fig. 6). Since these magnon excitations are bosonic, they occur at the finite energies. These topological magnons [81–87] are magnetic analogues of the electronic topological semimetals [88, 89].

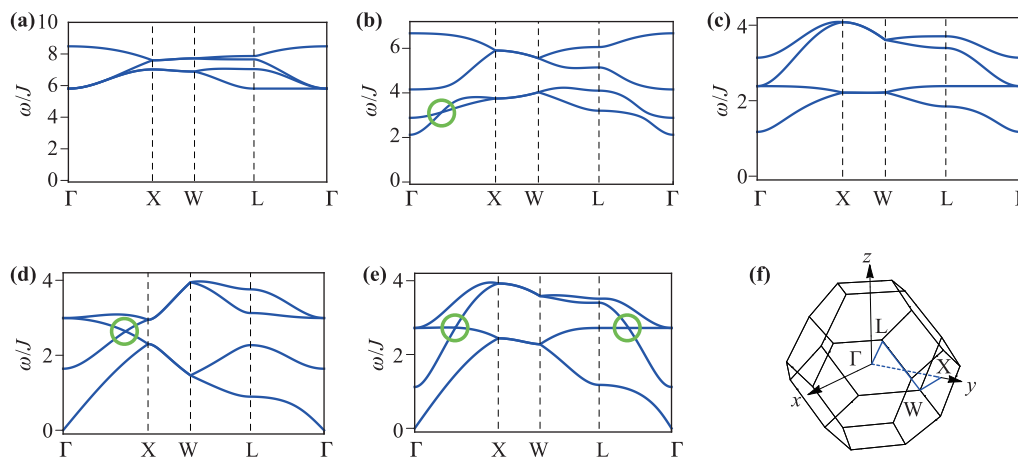


**Fig. 5** Spin wave excitations of the ordered phases. The parameters are chosen as (a)  $D = -J, D_z = 0$  (all-in all-out); (b)  $D = J, D_z = -0.3J$  (splayed FM, the ferromagnetic component is set along the global  $\hat{z}$  direction); (c)  $D = -0.3J, D_z = 0.6J$  (coplanar XY AFM<sub>1</sub>, the configuration is set on the global  $xy$  plane); (d)  $D = 0.1J, D_z = J, \theta = \pi/3$  (non-coplanar XY AFM); (e)  $D = 0.5J, D_z = 0.1J, \theta = 5\pi/6$  (coplanar XY AFM<sub>2</sub>). We plot the Brillouin zone of the pyrochlore lattice and indicate the high symmetry lines in (f). Green circles in (b), (d), and (e) indicate band touchings belong to certain nodal lines, shown in Fig. 6.

## 5 Summary with a materials' survey

In this short review, we systematically discussed a generic spin model that can describe the interacting spin-1 moments on a pyrochlore lattice. We have explained the global phase diagram with very rich phases for this generic spin model with several different and complementary approaches. The magnetic ordered states are understood from both the mean-field theory and the instability of the quantum paramagnetic phase. The relations between different phases are further clarified. Both the magnetic structures of the ordered phases and the corresponding elementary excitations are carefully studied. The existence of degenerate and topological excitations are also discussed. While these results are valid within the approximation, one expects that the results break down when the system approaches the Heisenberg limit of the spin-1 model. Thus, the phases in the vicinity of the Heisenberg model of Fig. 1 are expected to be altered, and more quantum treatment is needed. The ground state for the pyrochlore lattice Heisenberg model is one of the hardest problems in quantum magnetism. The early theoretical attempts provide insights for the classical limit [90, 91]. Due to the extensive classical ground state degeneracy there, the quantum fluctuation is deemed to be very strong when the quantum nature of the spins is considered. Moreover, there should be fundamental distinctions between the spin-1/2 and the spin-1 Heisenberg models.

Finally, we give a list of candidate spin-1 pyrochlore materials in Table 1 and explain their physical properties to end this review. There have already been several spin-1 pyrochlore materials in the literature. We start from the

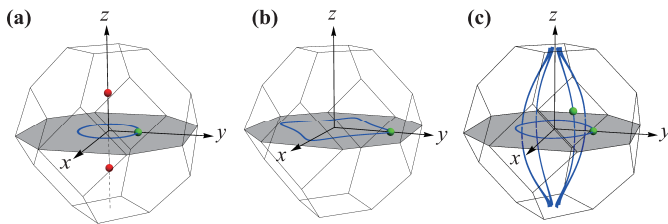


**Fig. 6** The nodal lines and Weyl nodes of the spin wave excitation. **(a)** For the same parameters as in Fig. 5(b), there is a nodal contour on the (001) plane (gray) of the reciprocal space. The band touching shown in Fig. 5(b) is indicated by a green dot here. Moreover, there exists a pair of Weyl nodes along  $z$  axis, indicated by red dots. **(b)** For the same parameters as in Fig. 5(d), there is a nodal contour on the (001) plane (gray) of the reciprocal space too. Again the band touching shown in Fig. 5(d) is indicated by a green dot. **(c)** For the same parameters as in Fig. 5(e), the nodal lines form a cage-like structure. One nodal contour is located on the (001) plane (gray) and intersects with the other four nodal lines, of which two are located on the (110) plane and the other two are located on the (1 $\bar{1}$ 0) plane. The two band touchings shown in Fig. 5(e) are indicated by green dots.

Ni-based pyrochlore material  $\text{NaCaNi}_2\text{F}_7$  [66]. This material has a  $-129$  K Curie–Weiss temperature, and no features of spin orderings are observed in the thermodynamic measurement until a spin glassy transition at 3.6 K. The spin glassy transition is evidenced by the bifurcation in the magnetic susceptibility between the zero-field-cooled and field-cooled results. The magnetic entropy saturates to  $R\ln 2$  when the temperature is increased to 70 K [66]. The highest temperature 70 K in the entropy measurement is probably not too large to exhaust the actual magnetic entropy as the Curie–Weiss temperature is  $-129$  K. If one takes this entropy result, this magnetic entropy differs from the simple expectation for the spin-1 local moment and indicates a significant easy-axis spin anisotropy that reduces the total magnetic entropy. In this case, based on the phase diagram in Fig. 1, there would be magnetic orders. It is possible that the exchange randomness becomes important at low temperatures and drives the system into a spin glassy state instead. Since the glassy transition occurs at very low temperatures, the spin physics and dynamics at higher temperatures and energy scales are probably less influenced by the exchange randomness. If the current entropy result is not reliable due to the small upper temperature limit, one could extend the entropy measurement further in the temperature to see if one can exhaust the spin-1 magnetic entropy. In any case, to test the relevance of the model Hamiltonian, it can be helpful to measure the spin correlation in the momentum space with neutron scattering and compare with the theoretical results. Since the generic spin model contains the spin space anisotropy in addition to the momentum space due to the single-ion anisotropy and Dzyaloshinskii–Moriya interaction, it is also quite useful to carry out the polarized neutron scattering measurement on the single-crystalline sample to detect the spin correlation function in the spin space. A very recent neutron scattering experiment was actually implemented on a single crystal sample. The general features of the spin correlation seem to be well captured by the first neighbor Heisenberg model with much weaker further neighbor interactions [113].

In fact, there exists a simple and useful recipe to estimate the Dzyaloshinskii–Moriya interaction but not the single-ion spin anisotropy. The effective magnetic moment of the Ni ion in  $\text{NaCaNi}_2\text{F}_7$  is found to be  $3.7\mu_B$  from the susceptibility data from 5 K to 300 K [66]. This deviates from  $2.82\mu_B$  for the pure  $S = 1$  moment in the atomic limit, and this deviation is due to the spin–orbit coupling. It is known that the deviation  $\Delta g$  of the Landé  $g$  factor is related to the Dzyaloshinskii–Moriya interaction [114] with  $\Delta g/g \sim |\mathbf{D}_{ij}|/J$ . This suggests that the Dzyaloshinskii–Moriya interaction may be up to 20%–30% of the Heisenberg exchange in  $\text{NaCaNi}_2\text{F}_7$ . This suggestion seems to be inconsistent with the conclusion that the system is described by the Heisenberg model in Ref. [113]. If the latter is true, there should be an unknown cancellation mechanism in the exchange paths that suppress the

**Table 1** A list of candidate spin-1 pyrochlore materials. The null entry means that the data is not available. A detailed discussion can be found in Ref. [71].

Materials	Magnetic ions	$\Theta_{CW}$	Magnetic transitions	Magnetic structure	Refs.
NaCaNi <sub>2</sub> F <sub>7</sub>	Ni <sup>2+</sup> (3d <sup>8</sup> )	-129 K	glassy transition at 3.6 K	spin glass	[66]
Y <sub>2</sub> Ru <sub>2</sub> O <sub>7</sub>	Ru <sup>4+</sup> (4d <sup>4</sup> )	-1250 K	AFM transition at 76 K	noncollinear AFM $\mathbf{Q} = \mathbf{0}$	[92]
Tl <sub>2</sub> Ru <sub>2</sub> O <sub>7</sub>	Ru <sup>4+</sup> (4d <sup>4</sup> )	-956 K	structure transition at 120 K	gapped paramagnet	[93]
Eu <sub>2</sub> Ru <sub>2</sub> O <sub>7</sub>	Ru <sup>4+</sup> (4d <sup>4</sup> )	—	Ru order at 118 K	Ru order	[94]
Pr <sub>2</sub> Ru <sub>2</sub> O <sub>7</sub>	Ru <sup>4+</sup> (4d <sup>4</sup> ), Pr <sup>3+</sup> (4f <sup>2</sup> )	-224 K	Ru AFM order at 162 K	Ru AFM order	[95, 96]
Nd <sub>2</sub> Ru <sub>2</sub> O <sub>7</sub>	Ru <sup>4+</sup> (4d <sup>4</sup> ), Nd <sup>3+</sup> (4f <sup>3</sup> )	-168 K	Ru AFM order at 143 K	Ru AFM order	[97]
Gd <sub>2</sub> Ru <sub>2</sub> O <sub>7</sub>	Ru <sup>4+</sup> (4d <sup>4</sup> ), Gd <sup>3+</sup> (4f <sup>7</sup> )	-10 K	Ru AFM order at 114 K	Ru AFM order $\mathbf{Q} = \mathbf{0}$	[98]
Tb <sub>2</sub> Ru <sub>2</sub> O <sub>7</sub>	Ru <sup>4+</sup> (4d <sup>4</sup> ), Tb <sup>3+</sup> (4f <sup>8</sup> )	-16 K	Ru AFM order at 110 K	Ru AFM order $\mathbf{Q} = \mathbf{0}$	[99]
Dy <sub>2</sub> Ru <sub>2</sub> O <sub>7</sub>	Ru <sup>4+</sup> (4d <sup>4</sup> ), Dy <sup>3+</sup> (4f <sup>9</sup> )	-10 K	Ru AFM order at 100 K	Ru AFM order	[100]
Ho <sub>2</sub> Ru <sub>2</sub> O <sub>7</sub>	Ru <sup>4+</sup> (4d <sup>4</sup> ), Ho <sup>3+</sup> (4f <sup>10</sup> )	-4 K	Ru AFM order at 95 K	Ru FM order $\mathbf{Q} = \mathbf{0}$	[101, 102]
Er <sub>2</sub> Ru <sub>2</sub> O <sub>7</sub>	Ru <sup>4+</sup> (4d <sup>4</sup> ), Er <sup>3+</sup> (4f <sup>11</sup> )	-16 K	Ru AFM order at 92 K	Ru AFM order $\mathbf{Q} = \mathbf{0}$	[103, 104]
Yb <sub>2</sub> Ru <sub>2</sub> O <sub>7</sub>	Ru <sup>4+</sup> (4d <sup>4</sup> ), Yb <sup>3+</sup> (4f <sup>13</sup> )	—	Ru AFM order at 83 K	Ru AFM order	[102]
Y <sub>2</sub> Mo <sub>2</sub> O <sub>7</sub>	Mo <sup>4+</sup> (4d <sup>2</sup> )	-200 K	Mo spin glass at 22 K	Mo spin glass	[105–108]
Lu <sub>2</sub> Mo <sub>2</sub> O <sub>7</sub>	Mo <sup>4+</sup> (4d <sup>2</sup> )	-160 K	Mo spin glass at 16 K	Mo spin glass	[109]
Tb <sub>2</sub> Mo <sub>2</sub> O <sub>7</sub>	Mo <sup>4+</sup> (4d <sup>2</sup> ), Tb <sup>3+</sup> (4f <sup>8</sup> )	20 K	spin glass at 25 K	spin glass	[110–112]

Dzyaloshinskii–Moriya interaction. If the Dzyaloshinskii–Moriya interaction is sizable, its effect would appear in the low-temperature magnetic properties.

Other existing spin-1 pyrochlore materials are the Ru-based pyrochlore A<sub>2</sub>Ru<sub>2</sub>O<sub>7</sub> and the Mo-based pyrochlore A<sub>2</sub>Mo<sub>2</sub>O<sub>7</sub>. Both of them are discussed and summarized in a very nice review paper [18] by Gardner, Gingras, and Greedan. In both systems, the A site can be a rare-earth ion or a non-magnetic ion with no moments. In the former case, the coupling between the rare-earth moments and the Ru/Mo moments may be important, and the rare-earth magnetism also contributes to the magnetic properties of the system. If the Ru–Ru interaction is the dominant one, one may first consider the magnetic physics of the Ru subsystem. In the latter case and also for A = Eu, one only needs to consider the Ru/Mo magnetism. The Ru<sup>4+</sup> ion has a 4d<sup>4</sup> electron configuration, and the electrons occupy the lower t<sub>2g</sub> orbitals. Although the atomic spin–orbit coupling is still active due to the partially filled t<sub>2g</sub> manifold, the Hund’s coupling could suppress the effect

from the spin–orbit coupling for the 4d<sup>4</sup> electron configuration. If the spin–orbit coupling is truly dominant over the Hund’s coupling, a quenched local moment would be obtained. Since these are 4d electrons, we expect the spin–orbit coupling could just be moderate compared to the Hund’s coupling. From the experimental result of a spin-1 moment for the Ru<sup>4+</sup> ion, it is reasonable to take the view of a moderate spin–orbit coupling. Moreover, as it is shown in Fig. 7, there can be two different occupation configurations after one includes the trigonal distortion. Fig. 7(a) has an orbital degeneracy, while Fig. 7(b) has no orbital degeneracy. The prevailing view of spin-only moment [18] for the Ru<sup>4+</sup> ion supports the choice of Fig. 7(b). Moreover, due to different orbital occupation configurations and the realization of the spin–orbit coupling for the Ru<sup>4+</sup> ion, although the model stays the same as Eq. (1), the single-ion anisotropy and the Dzyaloshinskii–Moriya interaction would have different relations from the ones in Eq. (2) and Eq. (3).

As we show in Table 1, almost all materials in

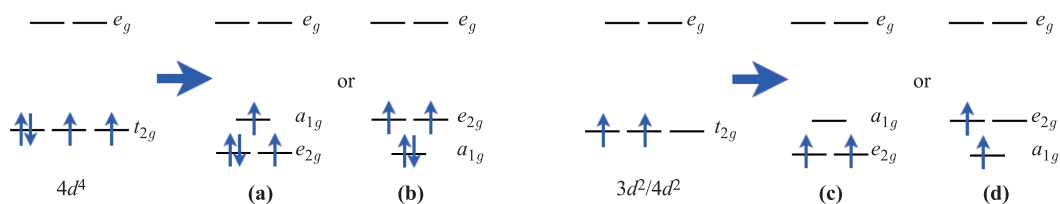


**Fig. 7** Left: The orbital occupations for 4d<sup>4</sup> electron configuration. Under the trigonal distortion, the threefold degenerate t<sub>2g</sub> orbitals are splitted into a<sub>1g</sub> and twofold degenerate e<sub>2g</sub> states. There are two possible electron occupation configurations: (a) has an unquenched orbital degree of freedom and (b) does not have. Right: The orbital occupations for 3d<sup>2</sup>/4d<sup>2</sup> electron configuration. Again under the trigonal distortion, the threefold degenerate t<sub>2g</sub> orbitals are splitted into a<sub>1g</sub> and twofold degenerate e<sub>2g</sub> states. In the two possible electron occupation configurations, (d) has an unquenched orbital degree of freedom and (c) does not have.

the  $A_2Ru_2O_7$  family develop magnetic orders except  $Tl_2Ru_2O_7$ . We start from the materials with pure Ru moments. The non-collinear AFM state, that was found for  $Y_2Ru_2O_7$  in Ref. [92], is simply the coplanar XY AFM<sub>1</sub> state in Fig. 4. It is thus of interest to search for topological magnons in this material.  $Tl_2Ru_2O_7$  experiences a structural transition at 120 K that breaks the cubic symmetry, so our model does not really apply here.  $Eu_2Ru_2O_7$  was suggested to develop Ru sublattice orders at 118 K and experience a glassy-like transition at 23 K [94]. The precise nature of the Ru order is not known. The Ru materials with the unquenched rare-earth moments contain richer physics than the ones with non-magnetic rare-earth moments. There are three energy scales to consider. From high to low in the energy scales, one would list them as Ru–Ru exchange interaction,  $f$ – $d$  exchange between the Ru moments and rare-earth moments, and the exchange and dipolar interactions between the rare-earth moments. This hierarchical energy structure arises from the different spatial extension of the  $4d$  electrons and the  $4f$  electrons. Since the Ru–Ru exchange interaction would be the dominant one, we would expect the Ru moments to develop structures at higher temperatures and influence the rare-earth moments via the  $f$ – $d$  exchange. The existing experiments support this view [18]. The experimental study on these rare-earth based Ru pyrochlores has not been quite systematic yet. Only limited experimental information is available. We here restrict the discussion to the systems with more known results.  $Ho_2Ru_2O_7$  was studied using neutron scattering measurements in a nice paper [101] by Wiebe *et al.*. The authors revealed the Ru moment order at  $\sim 95$  K and the Ho moment order at  $\sim 1.4$  K. The high temperature Ru magnetic order is consistent with the splayed FM with a splayed angle  $\alpha \approx 41^\circ$ . Under the internal exchange field from the Ru order, the Ho moment further develops a magnetic order at a lower temperature. Despite the agreement between the experimental order and theoretical result, further measurement of the magnetic excitation within the splayed FM can be useful to identify nontrivial magnon modes. Ref. [104] carried out a powder neutron scattering measurement on  $Er_2Ru_2O_7$  and proposed a  $\mathbf{Q} = \mathbf{0}$  ordered state with a collinear antiferromagnetic magnetic order along the  $\langle 001 \rangle$  lattice direction for the Ru moments. Like  $Ho_2Ru_2O_7$ , the Er moments develop a magnetic order at a much lower temperature while the Ru moment ordering occurs at a higher temperature and should be understood first. To stabilize the collinear order for the Ru moments, one may need a bi-quadratic spin interaction [115, 116]. This collinear state is actually not among the ordered states in the phase diagram of Fig. 1. However, it is suspected that one ordered state in Fig. 4, especially the coplanar XY AFM<sub>2</sub> state or the non-coplanar XY AFM state, may also explain the existing data, e.g., observed magnetic reflection intensities, for  $Er_2Ru_2O_7$ . More experiments are needed to sort out the actual magnetic order in this material. Because the Ru

spin-1 moments in these materials often order at a higher temperature, it would be interesting to examine the precise magnetic structure and the magnetic excitations in the future experiments and compare with the theoretical prediction. Future directions in these materials should at least include the understanding of the  $f$ – $d$  exchange between the rare-earth moments and the Ru moments and the magnetic properties of the rare-earth subsystem. The  $f$ – $d$  exchange significantly depends on the nature of the rare-earth moment, i.e., whether it is Kramers doublet, non-Kramers doublet or dipole–octupole doublet. As a result, the Ru molecular or internal exchange field on the rare-earth subsystem not only depends on the magnetic structure of the Ru subsystem, but also depends on the form of the  $f$ – $d$  exchange. This may give rise to rich magnetic structures and properties on the rare-earth subsystems in the ordered phase of the Ru subsystems.

It is interesting to compare the spin-1 Ru pyrochlores with the rare-earth osmates ( $A_2Os_2O_7$ ) and molybdates ( $A_2Mo_2O_7$ ). The  $Os^{4+}$  ion has a  $5d^4$  electron configuration, and spin–orbit coupling is stronger than  $Ru^{4+}$ . As a result, rather than forming a  $S = 1$  local moment, the magnetic moment of the  $Os^{4+}$  ion is strongly suppressed by the spin–orbit coupling that would favor a spin–orbital singlet in the strong spin–orbit coupling limit [117–119]. Unlike the insulating Ru-based pyrochlores, most Mo-based pyrochlore materials are metallic [18]. The  $Mo^{4+}$  has a  $4d^2$  electron configuration. The metallic behavior is probably because the Hund’s coupling suppresses the correlation effect and induces Hund’s metals [120]. Instead of developing magnetic orders, the insulating ones ( $Y_2Mo_2O_7$ ,  $Lu_2Mo_2O_7$ , and  $Tb_2Mo_2O_7$ ) all show spin glassy behaviors. The origin of the spin glass in these geometrically frustrated pyrochlore molybdates remains to be a puzzle in the field [18]. It is possible that, the orbital occupation of the  $Mo^{4+}$  ion is not given by Fig. 7(c) and is instead given by Fig. 7(d). In that case, the Mo local moment contains a unquenched orbital degree of freedom, and the orbital and spin interact in a Kugel-Khomskii fashion [121] and are affected by the lattice phonons. This spin–orbital physics has been suggested for the spinel vanadate  $AV_2O_4$  ( $A = Ca, Mg, Cd, Zn$ ), where  $V^{3+}$ :  $3d^2$  was expected to take the electron configuration in Fig. 7(d) [122–127] and forms a spin-1 pyrochlore system with additional orbital degree of freedom.

**Acknowledgements** This work was supported by the Ministry of Science and Technology of China with grant Nos. 2016YFA0301001, 2016YFA0300501, and 2018YFE0103200, and the General Research Fund (GRF) under grant No. 17303819 from the Research Grant Council of Hong Kong.

## References

1. F. D. M. Haldane, Nonlinear field theory of large-spin Heisenberg antiferromagnets: Semiclassically quantized

- solitons of the one-dimensional easy-axis Néel state, *Phys. Rev. Lett.* 50(15), 1153 (1983)
2. F. Haldane, Continuum dynamics of the 1-D Heisenberg antiferromagnet: Identification with the O(3) nonlinear sigma model, *Phys. Lett. A* 93(9), 464 (1983)
  3. I. Affleck, T. Kennedy, E. H. Lieb, and H. Tasaki, Rigorous results on valence-bond ground states in antiferromagnets, *Phys. Rev. Lett.* 59(7), 799 (1987)
  4. X. Chen, Z. C. Gu, and X. G. Wen, Classification of gapped symmetric phases in one-dimensional spin systems, *Phys. Rev. B* 83(3), 035107 (2011)
  5. C. Wang, A. Nahum, and T. Senthil, Topological paramagnetism in frustrated spin-1 Mott insulators, *Phys. Rev. B* 91(19), 195131 (2015)
  6. G. Chen, Quantum paramagnet and frustrated quantum criticality in a spin-one diamond lattice antiferromagnet, *Phys. Rev. B* 96(2), 020412 (2017)
  7. L. Savary, Quantum loop states in spin-orbital models on the honeycomb lattice, arXiv: 1511.01505 (2015)
  8. Z. Wang, A. E. Feiguin, W. Zhu, O. A. Starykh, A. V. Chubukov, and C. D. Batista, Chiral liquid phase of simple quantum magnets, *Phys. Rev. B* 96(18), 184409 (2017)
  9. F. L. Buessen, M. Hering, J. Reuther, and S. Trebst, Quantum spin liquids in frustrated spin-1 diamond antiferromagnets, arXiv: 1706.06299 (2017)
  10. J. R. Chamorro, L. Ge, J. Flynn, M. A. Subramanian, M. Mourigal, and T. M. McQueen, Frustrated spin one on a diamond lattice in NiRh<sub>2</sub>O<sub>4</sub>, *Phys. Rev. Mater.* 2(3), 034404 (2018)
  11. J. G. Cheng, G. Li, L. Balicas, J. S. Zhou, J. B. Goodenough, C. Xu, and H. D. Zhou, High-pressure sequence of Ba<sub>3</sub>NiSb<sub>2</sub>O<sub>9</sub> structural phases: New  $S = 1$  quantum spin liquids based on Ni<sup>2+</sup>, *Phys. Rev. Lett.* 107(19), 197204 (2011)
  12. M. Serbyn, T. Senthil, and P. A. Lee, Exotic  $S = 1$  spin-liquid state with fermionic excitations on the triangular lattice, *Phys. Rev. B* 84(18), 180403 (2011)
  13. S. Bieri, M. Serbyn, T. Senthil, and P. A. Lee, Paired chiral spin liquid with a Fermi surface in  $S = 1$  model on the triangular lattice, *Phys. Rev. B* 86(22), 224409 (2012)
  14. C. Xu, F. Wang, Y. Qi, L. Balents, and M. P. A. Fisher, Spin liquid phases for spin-1 systems on the triangular lattice, *Phys. Rev. Lett.* 108(8), 087204 (2012)
  15. G. Chen, M. Hermele, and L. Radzihovsky, Frustrated quantum critical theory of putative spin-liquid phenomenology in 6H-B-Ba<sub>3</sub>NiSb<sub>2</sub>O<sub>9</sub>, *Phys. Rev. Lett.* 109(1), 016402 (2012)
  16. K. Hwang, T. Dodds, S. Bhattacharjee, and Y. B. Kim, Three-dimensional nematic spin liquid in a stacked triangular lattice 6H-B structure, *Phys. Rev. B* 87(23), 235103 (2013)
  17. J. A. Quilliam, F. Bert, A. Manseau, C. Darie, C. Guillot-Deudon, C. Payen, C. Baines, A. Amato, and P. Mendels, Gapless quantum spin liquid ground state in the spin-1 antiferromagnet 6HB-Ba<sub>3</sub>NiSb<sub>2</sub>O<sub>9</sub>, *Phys. Rev. B* 93(21), 214432 (2016)
  18. J. S. Gardner, M. J. P. Gingras, and J. E. Greedan, Magnetic pyrochlore oxides, *Rev. Mod. Phys.* 82(1), 53 (2010)
  19. S. T. Bramwell and M. J. P. Gingras, Spin ice state in frustrated magnetic pyrochlore materials, *Science* 294(5546), 1495 (2001)
  20. R. G. Melko, B. C. den Hertog, and M. J. P. Gingras, Long-range order at low temperatures in dipolar spin ice, *Phys. Rev. Lett.* 87(6), 067203 (2001)
  21. C. Castelnovo, R. Moessner, and S. L. Sondhi, Magnetic monopoles in spin ice, *Nature* 451(7174), 42 (2008)
  22. H. R. Molavian, M. J. P. Gingras, and B. Canals, Dynamically induced frustration as a route to a quantum spin ice state in Tb<sub>2</sub>Ti<sub>2</sub>O<sub>7</sub> via virtual crystal field excitations and quantum many-body effects, *Phys. Rev. Lett.* 98(15), 157204 (2007)
  23. M. J. P. Gingras and P. A. McClarty, Quantum spin ice: A search for gapless quantum spin liquids in pyrochlore magnets, *Rep. Prog. Phys.* 77(5), 056501 (2014)
  24. L. Savary and L. Balents, Quantum spin liquids: A review, *Rep. Prog. Phys.* 80(1), 016502 (2017)
  25. S. Onoda and Y. Tanaka, Quantum melting of spin ice: Emergent cooperative quadrupole and chirality, *Phys. Rev. Lett.* 105(4), 047201 (2010)
  26. L. Savary and L. Balents, Coulombic quantum liquids in spin-1/2 pyrochlores, *Phys. Rev. Lett.* 108(3), 037202 (2012)
  27. S. Lee, S. Onoda, and L. Balents, Generic quantum spin ice, *Phys. Rev. B* 86(10), 104412 (2012)
  28. L. Savary and L. Balents, Spin liquid regimes at nonzero temperature in quantum spin ice, *Phys. Rev. B* 87(20), 205130 (2013)
  29. H. Fukazawa, R. G. Melko, R. Higashinaka, Y. Maeno, and M. J. P. Gingras, Magnetic anisotropy of the spin-ice compound Dy<sub>2</sub>Ti<sub>2</sub>O<sub>7</sub>, *Phys. Rev. B* 65(5), 054410 (2002)
  30. S. T. Bramwell, M. J. Harris, B. C. den Hertog, M. J. P. Gingras, J. S. Gardner, D. F. McMorrow, A. R. Wildes, A. L. Cornelius, J. D. M. Champion, R. G. Melko, and T. Fennell, Spin correlations in Ho<sub>2</sub>Ti<sub>2</sub>O<sub>7</sub>: A dipolar spin ice system, *Phys. Rev. Lett.* 87(4), 047205 (2001)
  31. K. A. Ross, J. P. C. Ruff, C. P. Adams, J. S. Gardner, H. A. Dabkowska, Y. Qiu, J. R. D. Copley, and B. D. Gaulin, Two-dimensional Kagome correlations and field induced order in the ferromagnetic XY pyrochlore Yb<sub>2</sub>Ti<sub>2</sub>O<sub>7</sub>, *Phys. Rev. Lett.* 103(22), 227202 (2009)
  32. Y. P. Huang, G. Chen, and M. Hermele, Quantum spin ices and topological phases from dipolar-octupolar doublets on the pyrochlore lattice, *Phys. Rev. Lett.* 112(16), 167203 (2014)
  33. G. Chen, “Magnetic monopole” condensation of the pyrochlore ice  $U(1)$  quantum spin liquid: Application to Pr<sub>2</sub>Ir<sub>2</sub>O<sub>7</sub> and Yb<sub>2</sub>Ti<sub>2</sub>O<sub>7</sub>, *Phys. Rev. B* 94(20), 205107 (2016)
  34. Y. Wan and O. Tchernyshyov, Quantum strings in quantum spin ice, *Phys. Rev. Lett.* 108(24), 247210 (2012)
  35. Y. D. Li and G. Chen, Symmetry enriched  $U(1)$  topological orders for dipole-octupole doublets on a pyrochlore lattice, *Phys. Rev. B* 95(4), 041106 (2017)

36. H. Yan, O. Benton, L. Jaubert, and N. Shannon, Theory of multiple-phase competition in pyrochlore magnets with anisotropic exchange with application to  $\text{Yb}_2\text{Ti}_2\text{O}_7$ ,  $\text{Er}_2\text{Ti}_2\text{O}_7$ , and  $\text{Er}_2\text{Sn}_2\text{O}_7$ , *Phys. Rev. B* 95(9), 094422 (2017)
37. L. Savary, X. Wang, H. Y. Kee, Y. B. Kim, Y. Yu, and G. Chen, Quantum spin ice on the breathing pyrochlore lattice, *Phys. Rev. B* 94(7), 075146 (2016)
38. T. Fennell, M. Kenzelmann, B. Roessli, M. K. Haas, and R. J. Cava, Power-law spin correlations in the pyrochlore antiferromagnet  $\text{Tb}_2\text{Ti}_2\text{O}_7$ , *Phys. Rev. Lett.* 109(1), 017201 (2012)
39. Y. Yasui, M. Kanada, M. Ito, H. Harashina, M. Sato, H. Okumura, K. Kakurai, and H. Kadowaki, Static correlation and dynamical properties of  $\text{Tb}^{3+}$ -moments in  $\text{Tb}_2\text{Ti}_2\text{O}_7$  – neutron scattering study, *J. Phys. Soc. Jpn.* 71(2), 599 (2002)
40. J. S. Gardner, B. D. Gaulin, A. J. Berlinsky, P. Waldron, S. R. Dunsiger, N. P. Raju, and J. E. Greedan, Neutron scattering studies of the cooperative paramagnet pyrochlore  $\text{Tb}_2\text{Ti}_2\text{O}_7$ , *Phys. Rev. B* 64(22), 224416 (2001)
41. Z. Hao, A. G. R. Day, and M. J. P. Gingras, Bosonic many-body theory of quantum spin ice, *Phys. Rev. B* 90(21), 214430 (2014)
42. L. J. Chang, S. Onoda, Y. Su, Y. J. Kao, K. D. Tsuei, Y. Yasui, K. Kakurai, and M. R. Lees, Higgs transition from a magnetic Coulomb liquid to a ferromagnet in  $\text{Yb}_2\text{Ti}_2\text{O}_7$ , *Nat. Commun.* 3(1), 992 (2012)
43. K. Kimura, K. Nakatsuji, J. J. Wen, C. Broholm, M. Stone, E. Nishibori, and H. Sawa, Quantum fluctuations in spin-ice-like  $\text{Pr}_2\text{Zr}_2\text{O}_7$ , *Nat. Commun.* 4(1), 1934 (2013)
44. E. Lhotel, S. R. Giblin, M. R. Lees, G. Balakrishnan, L. J. Chang, and Y. Yasui, First-order magnetic transition in  $\text{Yb}_2\text{Ti}_2\text{O}_7$ , *Phys. Rev. B* 89(22), 224419 (2014)
45. L.J. Chang, M. R. Lees, I. Watanabe, A. D. Hillier, Y. Yasui, and S. Onoda, Static magnetic moments revealed by muon spin relaxation and thermodynamic measurements in the quantum spin ice  $\text{Yb}_2\text{Ti}_2\text{O}_7$ , *Phys. Rev. B* 89(18), 184416 (2014)
46. Y. Yasui, M. Soda, S. Iikubo, M. Ito, M. Sato, N. Hamaguchi, T. Matsushita, N. Wada, T. Takeuchi, N. Aso, and K. Kakurai, Ferromagnetic transition of pyrochlore compound  $\text{Yb}_2\text{Ti}_2\text{O}_7$ , *J. Phys. Soc. Jpn.* 72(11), 3014 (2003)
47. K. Ross, L. Savary, B. Gaulin, and L. Balents, Quantum excitations in quantum spin ice, *Phys. Rev. X* 1(2), 021002 (2011)
48. N. Shannon, O. Sikora, F. Pollmann, K. Penc, and P. Fulde, Quantum ice: A quantum Monte Carlo study, *Phys. Rev. Lett.* 108(6), 067204 (2012)
49. P. Goswami, B. Roy, and S. Das Sarma, Itinerant spin ice order, Weyl metal, and anomalous Hall effect in  $\text{Pr}_2\text{Ir}_2\text{O}_7$ , arXiv: 1603.02273 (2016)
50. K. E. Arpino, B. A. Trump, A. O. Scheie, T. M. McQueen, and S. M. Koohpayeh, Impact of stoichiometry of  $\text{Yb}_2\text{Ti}_2\text{O}_7$  on its physical properties, *Phys. Rev. B* 95(9), 094407 (2017)
51. J. J. Wen, S. M. Koohpayeh, K. A. Ross, B. A. Trump, T. M. McQueen, K. Kimura, S. Nakatsuji, Y. Qiu, D. M. Pajerowski, J. R. D. Copley, and C. L. Broholm, Disordered route to the Coulomb quantum spin liquid: Random transverse fields on spin ice in  $\text{Pr}_2\text{Zr}_2\text{O}_7$ , *Phys. Rev. Lett.* 118(10), 107206 (2017)
52. D. E. MacLaughlin, O. O. Bernal, L. Shu, J. Ishikawa, Y. Matsumoto, J. J. Wen, M. Mourigal, C. Stock, G. Ehlers, C. L. Broholm, Y. Machida, K. Kimura, S. Nakatsuji, Y. Shimura, and T. Sakakibara, Unstable spin-ice order in the stuffed metallic pyrochlore  $\text{Pr}_{2+x}\text{Ir}_{2-x}\text{O}_{7-\delta}$ , *Phys. Rev. B* 92(5), 054432 (2015)
53. G. Chen, H. Y. Kee, and Y. B. Kim, Fractionalized charge excitations in a spin liquid on partially filled pyrochlore lattices, *Phys. Rev. Lett.* 113(19), 197202 (2014)
54. J. Fu, J. G. Rau, M. J. Gingras, and N. B. Perkins, Fingerprints of quantum spin ice in Raman scattering, arXiv: 1703.03836 (2017)
55. O. Benton, O. Sikora, and N. Shannon, Seeing the light: Experimental signatures of emergent electromagnetism in a quantum spin ice, *Phys. Rev. B* 86(7), 075154 (2012)
56. L. D. C. Jaubert, O. Benton, J. G. Rau, J. Oitmaa, R. R. P. Singh, N. Shannon, and M. J. P. Gingras, Are multi-phase competition and order by disorder the keys to understanding  $\text{Yb}_2\text{Ti}_2\text{O}_7$ ? *Phys. Rev. Lett.* 115(26), 267208 (2015)
57. R. Applegate, N. R. Hayre, R. R. P. Singh, T. Lin, A. G. R. Day, and M. J. P. Gingras, Vindication of  $\text{Yb}_2\text{Ti}_2\text{O}_7$  as a model exchange quantum spin ice, *Phys. Rev. Lett.* 109(9), 097205 (2012)
58. S. R. Dunsiger, A. A. Aczel, C. Arguello, H. Dabkowska, A. Dabkowski, M. H. Du, T. Goko, B. Javanparast, T. Lin, F. L. Ning, H. M. L. Noad, D. J. Singh, T. J. Williams, Y. J. Uemura, M. J. P. Gingras, and G. M. Luke, Spin ice: Magnetic excitations without monopole signatures using muon spin rotation, *Phys. Rev. Lett.* 107(20), 207207 (2011)
59. R. Sibille, E. Lhotel, V. Pomjakushin, C. Baines, T. Fennell, and M. Kenzelmann, Candidate quantum spin liquid in the  $\text{Ce}^{3+}$  pyrochlore stannate  $\text{Ce}_2\text{Sn}_2\text{O}_7$ , *Phys. Rev. Lett.* 115(9), 097202 (2015)
60. M. Taillefumier, O. Benton, H. Yan, L. D. C. Jaubert, and N. Shannon, Competing spin liquids and hidden spin-nematic order in spin ice with frustrated transverse exchange, *Phys. Rev. X* 7(4), 041057 (2017)
61. G. Chen, Spectral periodicity of the spinon continuum in quantum spin ice, *Phys. Rev. B* 96(8), 085136 (2017)
62. L. Savary and L. Balents, Disorder-induced quantum spin liquid in spin ice pyrochlores, *Phys. Rev. Lett.* 118(8), 087203 (2017)
63. G. Chen, Dirac's "magnetic monopoles" in pyrochlore ice  $U(1)$  spin liquids: Spectrum and classification, *Phys. Rev. B* 96(19), 195127 (2017)

64. S. H. Curnoe, Structural distortion and the spin liquid state in  $\text{Tb}_2\text{Ti}_2\text{O}_7$ , *Phys. Rev. B* 78(9), 094418 (2008)
65. S. Onoda, Effective quantum pseudospin-1/2 model for Yb pyrochlore oxides, *J. Phys.: Conf. Ser.* 320, 012065 (2011)
66. J. W. Krizan and R. J. Cava,  $\text{NaCaNi}_2\text{F}_7$ : A single-crystal high-temperature pyrochlore antiferromagnet with  $S = 1 \text{ Ni}^{2+}$ , *Phys. Rev. B* 92, 014406 (2015)
67. J. W. Krizan and R. J. Cava,  $\text{NaCaCo}_2\text{F}_7$ : A single-crystal high-temperature pyrochlore antiferromagnet, *Phys. Rev. B* 89(21), 214401 (2014)
68. K. A. Ross, J. M. Brown, R. J. Cava, J. W. Krizan, S. E. Nagler, J. A. Rodriguez-Rivera, and M. B. Stone, Single-ion properties of the  $S_{\text{eff}} = 1/2$  XY antiferromagnetic pyrochlores  $\text{NaA}'\text{Co}_2\text{F}_7$  ( $A' = \text{Ca}^{2+}, \text{Sr}^{2+}$ ), *Phys. Rev. B* 95(14), 144414 (2017)
69. M. B. Sanders, J. W. Krizan, K. W. Plumb, T. M. McQueen, and R. J. Cava,  $\text{NaSrMn}_2\text{F}_7$ ,  $\text{NaCaFe}_2\text{F}_7$ , and  $\text{NaSrFe}_2\text{F}_7$ : Novel single crystal pyrochlore antiferromagnets, *J. Phys.: Condens. Matter* 29(4), 045801 (2017)
70. W. Witczak-Krempa, G. Chen, Y. B. Kim, and L. Balents, Correlated quantum phenomena in the strong spin-orbit regime, *Annu. Rev. Condens. Matter Phys.* 5(1), 57 (2014)
71. F. Y. Li and G. Chen, Competing phases and topological excitations of spin-1 pyrochlore antiferromagnets, *Phys. Rev. B* 98(4), 045109 (2018)
72. M. Elhajal, B. Canals, R. Sunyer, and C. Lacroix, Ordering in the pyrochlore antiferromagnet due to Dzyaloshinsky–Moriya interactions, *Phys. Rev. B* 71(9), 094420 (2005)
73. S. Maekawa, T. Tohyama, S. Barnes, S. Ishihara, W. Koshibae, and G. Khaliullin, *Physics of Transition Metal Oxides*, Springer, 2004
74. A. Joshi, M. Ma, F. Mila, D. N. Shi, and F. C. Zhang, Elementary excitations in magnetically ordered systems with orbital degeneracy, *Phys. Rev. B* 60(9), 6584 (1999)
75. Y. Q. Li, M. Ma, D. N. Shi, and F. C. Zhang,  $SU(4)$  theory for spin systems with orbital degeneracy, *Phys. Rev. Lett.* 81(16), 3527 (1998)
76. S. E. Palmer and J. T. Chalker, Order induced by dipolar interactions in a geometrically frustrated antiferromagnet, *Phys. Rev. B* 62(1), 488 (2000)
77. A. Poole, A. S. Wills, and E. Lelièvre-Berna, Magnetic ordering in the XY pyrochlore antiferromagnet  $\text{Er}_2\text{Ti}_2\text{O}_7$ : A spherical neutron polarimetry study, *J. Phys.: Condens. Matter* 19(45), 452201 (2007)
78. L. Savary, K. A. Ross, B. D. Gaulin, J. P. C. Ruff, and L. Balents, Order by quantum disorder in  $\text{Er}_2\text{Ti}_2\text{O}_7$ , *Phys. Rev. Lett.* 109(16), 167201 (2012)
79. M. E. Zhitomirsky, M. V. Gvozdikova, P. C. W. Holdsworth, and R. Moessner, Quantum order by disorder and accidental soft mode in  $\text{Er}_2\text{Ti}_2\text{O}_7$ , *Phys. Rev. Lett.* 109(7), 077204 (2012)
80. M. E. Zhitomirsky, P. C. W. Holdsworth, and R. Moessner, Nature of finite-temperature transition in anisotropic pyrochlore  $\text{Er}_2\text{Ti}_2\text{O}_7$ , *Phys. Rev. B* 89(14), 140403 (2014)
81. F. Y. Li, Y. D. Li, Y. B. Kim, L. Balents, Y. Yu, and G. Chen, Weyl magnons in breathing pyrochlore antiferromagnets, *Nat. Commun.* 7(1), 12691 (2016)
82. A. Mook, J. Henk, and I. Mertig, Tunable magnon Weyl points in ferromagnetic pyrochlores, *Phys. Rev. Lett.* 117(15), 157204 (2016)
83. F. Y. Li, Y. D. Li, Y. Yu, A. Paramakanti, and G. Chen, Kitaev materials beyond iridates: Order by quantum disorder and Weyl magnons in rare-earth double perovskites, *Phys. Rev. B* 95(8), 085132 (2017)
84. S. A. Owerre, Magnonic analogs of topological Dirac semimetals, *J. Phys. Commun.* 1(2), 025007 (2017)
85. S. A. Owerre, Topological magnetic excitations on the distorted Kagomé antiferromagnets: Applications to volborthite, vesignieite, and edwardsite, *EPL* 117(3), 37006 (2017)
86. J. Fransson, A. M. Black-Schaffer, and A. V. Balatsky, Magnon Dirac materials, *Phys. Rev. B* 94(7), 075401 (2016)
87. K. Li, C. Li, J. Hu, Y. Li, and C. Fang, Dirac and nodal line magnons in three-dimensional antiferromagnets, *Phys. Rev. Lett.* 119(24), 247202 (2017)
88. X. Wan, A. M. Turner, A. Vishwanath, and S. Y. Savrasov, Topological semimetal and Fermi-arc surface states in the electronic structure of pyrochlore iridates, *Phys. Rev. B* 83(20), 205101 (2011)
89. A. A. Burkov, M. D. Hook, and L. Balents, Topological nodal semimetals, *Phys. Rev. B* 84(23), 235126 (2011)
90. R. Moessner and J. T. Chalker, Low-temperature properties of classical geometrically frustrated antiferromagnets, *Phys. Rev. B* 58(18), 12049 (1998)
91. R. Moessner and J. T. Chalker, Properties of a classical spin liquid: The Heisenberg pyrochlore antiferromagnet, *Phys. Rev. Lett.* 80(13), 2929 (1998)
92. R. Kmiec, Z. Świątkowska, J. Gurgul, M. Rams, A. Zarzycki, and K. Tomala, Investigation of the magnetic properties of  $\text{Y}_2\text{Ru}_2\text{O}_7$  by  $^{99}\text{Ru}$  Mössbauer spectroscopy, *Phys. Rev. B* 74(10), 104425 (2006)
93. S. Lee, J. G. Park, D. T. Adroja, D. Khomskii, S. Streltsov, K. A. McEwen, H. Sakai, K. Yoshimura, V. I. Anisimov, D. Mori, R. Kanno, and R. Ibberson, Spin gap in  $\text{Tl}_2\text{Ru}_2\text{O}_7$  and the possible formation of Haldane chains in three-dimensional crystals, *Nat. Mater.* 5(6), 471 (2006)
94. S. M. PerezI, R. Cobas, J. M. Cadogan, J. A. Aguiar, C. Frontera, T. Puig, G. Long, M. DeMarco, D. Coffey, and X. Obradors, Anomalous electronic and magnetic properties of the  $\text{Eu}_2\text{Ru}_2\text{O}_7$  pyrochlore, *J. Appl. Phys.* 113, 17E102 (2013)
95. M. Tachibana, Heat capacity of pyrochlore  $\text{Pr}_2\text{Ru}_2\text{O}_7$ , *J. Appl. Phys.* 101, 09D502 (2007)
96. S. Zouari, R. Ballou, A. Cheikhrouhou, and P. Strobel, Structural and magnetic properties of the  $(\text{Bi}_{2-x}\text{Pr}_x)\text{Ru}_2\text{O}_7$  pyrochlore solid solution ( $0 \leq x \leq 2$ ), *J. Alloys Compd.* 476(1–2), 43 (2009)

97. M. W. Gaultois, P. T. Barton, C. S. Birkel, L. M. Misch, E. E. Rodriguez, G. D. Stucky, and R. Seshadri, Structural disorder, magnetism, and electrical and thermoelectric properties of pyrochlore  $\text{Nd}_2\text{Ru}_2\text{O}_7$ , *J. Phys.: Condens. Matter* 25(18), 186004 (2013)
98. J. Gurgul, M. Rams, Z. Świątkowska, R. Kmiec, and K. Tomala, Bulk magnetic measurements and  $^{99}\text{Ru}$  and  $^{155}\text{Gd}$  Mössbauer spectroscopies of  $\text{Gd}_2\text{Ru}_2\text{O}_7$ , *Phys. Rev. B* 75(6), 064426 (2007)
99. L. J. Chang, M. Prager, J. Perfon, J. Walter, E. Jansen, Y. Y. Chen, and J. S. Gardner, Magnetic order in the double pyrochlore  $\text{Tb}_2\text{Ru}_2\text{O}_7$ , *J. Phys.: Condens. Matter* 22(7), 076003 (2010)
100. Z. C. Xu, M. F. Liu, L. Lin, H. Liu, Z. B. Yan, and J. M. Liu, Experimental observations of ferroelectricity in double pyrochlore  $\text{Dy}_2\text{Ru}_2\text{O}_7$ , *Front. Phys.* 9(1), 82 (2014)
101. C. R. Wiebe, J. S. Gardner, S. J. Kim, G. M. Luke, A. S. Wills, B. D. Gaulin, J. E. Greedan, I. Swainson, Y. Qiu, and C. Y. Jones, Magnetic ordering in the spin-ice candidate  $\text{Ho}_2\text{Ru}_2\text{O}_7$ , *Phys. Rev. Lett.* 93(7), 076403 (2004)
102. N. Taira, M. Wakeshima, and Y. Hinatsu, Magnetic susceptibility and specific heat studies on heavy rare earth ruthenate pyrochlores  $\text{R}_2\text{Ru}_2\text{O}_7$  ( $\text{R} = \text{Gd}-\text{Yb}$ ), *J. Mater. Chem.* 12(5), 1475 (2002)
103. J. S. Gardner and G. Ehlers, Magnetic order and crystal field excitations in  $\text{Er}_2\text{Ru}_2\text{O}_7$ : A neutron scattering study, *J. Phys.: Condens. Matter* 21(43), 436004 (2009)
104. N. Taira, M. Wakeshima, Y. Hinatsu, A. Tobo, and K. Ohoyama, Magnetic structure of pyrochlore-type  $\text{Er}_2\text{Ru}_2\text{O}_7$ , *J. Solid State Chem.* 176(1), 165 (2003)
105. A. Keren and J. S. Gardner, Frustration driven lattice distortion: An NMR investigation of  $\text{Y}_2\text{Mo}_2\text{O}_7$ , *Phys. Rev. Lett.* 87(17), 177201 (2001)
106. P. M. M. Thygesen, J. A. M. Paddison, R. Zhang, K. A. Beyer, K. W. Chapman, H. Y. Playford, M. G. Tucker, D. A. Keen, M. A. Hayward, and A. L. Goodwin, Orbital dimer model for the spin-glass state in  $\text{Y}_2\text{Mo}_2\text{O}_7$ , *Phys. Rev. Lett.* 118(6), 067201 (2017)
107. H. J. Silverstein, K. Fritsch, F. Flicker, A. M. Hallas, J. S. Gardner, Y. Qiu, G. Ehlers, A. T. Savici, Z. Yamani, K. A. Ross, B. D. Gaulin, M. J. P. Gingras, J. A. M. Paddison, K. Foyevtsova, R. Valenti, F. Hawthorne, C. R. Wiebe, and H. D. Zhou, Liquidlike correlations in single-crystalline  $\text{Y}_2\text{Mo}_2\text{O}_7$ : An unconventional spin glass, *Phys. Rev. B* 89(5), 054433 (2014)
108. S. R. Dunsiger, R. F. Kiefl, K. H. Chow, B. D. Gaulin, M. J. P. Gingras, J. E. Greedan, A. Keren, K. Kojima, G. M. Luke, W. A. MacFarlane, N. P. Raju, J. E. Sonier, Y. J. Uemura, and W. D. Wu, Muon spin relaxation investigation of the spin dynamics of geometrically frustrated antiferromagnets  $\text{Y}_2\text{Mo}_2\text{O}_7$  and  $\text{Tb}_2\text{Mo}_2\text{O}_7$ , *Phys. Rev. B* 54(13), 9019 (1996)
109. L. Clark, G. J. Nilsen, E. Kermarrec, G. Ehlers, K. S. Knight, A. Harrison, J. P. Attfield, and B. D. Gaulin, From spin glass to quantum spin liquid ground states in molybdate pyrochlores, *Phys. Rev. Lett.* 113(11), 117201 (2014)
110. Y. Jiang, A. Huq, C. H. Booth, G. Ehlers, J. E. Greedan, and J. S. Gardner, Order and disorder in the local and long-range structure of the spin-glass pyrochlore,  $\text{Tb}_2\text{Mo}_2\text{O}_7$ , *J. Phys.: Condens. Matter* 23(16), 164214 (2011)
111. G. Ehlers, J. E. Greedan, J. R. Stewart, K. C. Rule, P. Fouquet, A. L. Cornelius, C. Adriano, P. G. Pagliuso, Y. Qiu, and J. S. Gardner, High-resolution neutron scattering study of  $\text{Tb}_2\text{Mo}_2\text{O}_7$ : A geometrically frustrated spin glass, *Phys. Rev. B* 81(22), 224405 (2010)
112. D. K. Singh, J. S. Helton, S. Chu, T. H. Han, C. J. Bonnoit, S. Chang, H. J. Kang, J. W. Lynn, and Y. S. Lee, Spin correlations in the geometrically frustrated pyrochlore  $\text{Tb}_2\text{Mo}_2\text{O}_7$ , *Phys. Rev. B* 78(22), 220405 (2008)
113. K. W. Plumb, H. J. Changlani, A. Scheie, S. Zhang, J. W. Krizan, J. A. Rodriguez-Rivera, Y. Qiu, B. Winn, R. J. Cava, and C. L. Broholm, Continuum of quantum fluctuations in a three-dimensional  $s = 1$  heisenberg magnet, arXiv: 1711.07509 (2017)
114. T. Moriya, Anisotropic superexchange interaction and weak ferromagnetism, *Phys. Rev.* 120(1), 91 (1960)
115. D. L. Bergman, R. Shindou, G. A. Fiete, and L. Balents, Models of degeneracy breaking in pyrochlore antiferromagnets, *Phys. Rev. B* 74(13), 134409 (2006)
116. K. Penc, N. Shannon, and H. Shiba, Half-magnetization plateau stabilized by structural distortion in the antiferromagnetic Heisenberg model on a pyrochlore lattice, *Phys. Rev. Lett.* 93(19), 197203 (2004)
117. G. Chen and L. Balents, Spin-orbit coupling in  $d^2$  ordered double perovskites, *Phys. Rev. B* 84(9), 094420 (2011)
118. Z. Y. Zhao, S. Calder, A. A. Aczel, M. A. McGuire, B. C. Sales, D. G. Mandrus, G. Chen, N. Trivedi, H. D. Zhou, and J. Q. Yan, Fragile singlet ground-state magnetism in the pyrochlore osmates  $\text{R}_2\text{Os}_2\text{O}_7$  ( $\text{R} = \text{Y}$  and  $\text{Ho}$ ), *Phys. Rev. B* 93(13), 134426 (2016)
119. G. Khaliullin, Excitonic magnetism in Van Vleck-type  $d^4$  Mott insulators, *Phys. Rev. Lett.* 111(19), 197201 (2013)
120. A. Georges, L. Medici, and J. Mravlje, Strong correlations from Hund's coupling, *Annu. Rev. Condens. Matter Phys.* 4(1), 137 (2013)
121. K. I. Kugel and D. I. Khomskii, The Jahn-Teller effect and magnetism: Transition metal compounds, *Sov. Phys. Usp.* 25(4), 231 (1982)
122. S. H. Lee, D. Louca, H. Ueda, S. Park, T. J. Sato, M. Isobe, Y. Ueda, S. Rosenkranz, P. Zschack, J. Íñiguez, Y. Qiu, and R. Osborn, Orbital and spin chains in  $\text{ZnV}_2\text{O}_4$ , *Phys. Rev. Lett.* 93(15), 156407 (2004)
123. T. Maitra and R. Valenti, Orbital order in  $\text{ZnV}_2\text{O}_4$ , *Phys. Rev. Lett.* 99(12), 126401 (2007)
124. G. Giovannetti, A. Stroppa, S. Picozzi, D. Baldomir, V. Pardo, S. Blanco-Canosa, F. Rivadulla, S. Jodlauk, D. Niermann, J. Rohrkamp, T. Lorenz, S. Streltsov, D. I. Khomskii, and J. Hemberger, Dielectric properties and magnetostriction of the collinear multiferroic spinel  $\text{CdV}_2\text{O}_4$ , *Phys. Rev. B* 83(6), 060402 (2011)

125. D. I. Khomskii and T. Mizokawa, Orbitally induced peierls state in spinels, *Phys. Rev. Lett.* 94(15), 156402 (2005)
126. S. Niitaka, H. Ohsumi, K. Sugimoto, S. Lee, Y. Oshima, K. Kato, D. Hashizume, T. Arima, M. Takata, and H. Takagi, A-type antiferro-orbital ordering with  $I4_1/a$  symmetry and geometrical frustration in the spinel vanadate  $\text{MgV}_2\text{O}_4$ , *Phys. Rev. Lett.* 111(26), 267201 (2013)
127. E. M. Wheeler, B. Lake, A. T. M. N. Islam, M. Reehuis, P. Steffens, T. Guidi, and A. H. Hill, Spin and orbital order in the vanadium spinel  $\text{MgV}_2\text{O}_4$ , *Phys. Rev. B* 82(14), 140406 (2010)